

Special
Collection

Bifunctional versus Defect-Mediated Effects in Electrocatalytic Methanol Oxidation

 Albert K. Engstfeld,^{*[a, b]} Jens Klein,^[a] and Sylvain Brimaud^[c]

The most prominent and intensively studied anode catalyst material for direct methanol oxidation fuel cells consists of a combination of platinum (Pt) and ruthenium (Ru). Classically, their high performance is attributed to a bifunctional reaction mechanism where Ru sites provide oxygen species at lower overpotential than Pt. In turn, they oxidize the adsorbed carbonaceous reaction intermediates at lower overpotential; among these, the Pt site-blocking carbon monoxide. We demonstrate that well-defined Pt modified Ru(0001) single crystal electrodes, with varying Pt contents and different local PtRu configurations at the surface, are unexpectedly inactive for the methanol oxidation reaction. This observation stands in contradiction with theoretical predictions and the concept of bifunctional catalysis for this reaction. Instead, we suggest that pure Pt defect sites play a more critical role than bifunctional defect sites on the electrodes investigated in this work.

The bimetallic combination platinum-ruthenium (PtRu) is a prominent and intensively studied bimetallic catalyst for their application as anode material in direct methanol fuel cells.^[1] The underlying electrocatalytic methanol oxidation reaction (MOR) does not necessarily proceed directly to CO₂. Instead a number of side products can form, i.e., formaldehyde, formic acid, methylformate or adsorbed CO, which remain as incomplete reaction products in the solution or adsorbed on the catalyst surface.^[2] Among these side reactions, a vital issue is the formation of strongly binding *CO as reaction intermediate, which acts as catalyst poison, significantly lowering the catalyst activity (the * denotes an adsorbed species throughout this

manuscript). Consequently, studies on both the MOR and the electrocatalytic CO oxidation reaction (COOR) received much attention over the last decades.^[1a,b] It is well established that the addition of Ru to the commonly employed bare Pt electrocatalyst material reduces the overpotential for the COOR and MOR. Historically, Watanabe and Motoo rationalized the performance improvements for this family of catalyst materials by a bifunctional Langmuir-Hinshelwood reaction mechanism.^[3] In this simple mechanistic picture, carbonaceous species adsorb preferentially on Pt sites, and the oxophilic Ru sites provide oxygen species (*OH/*O) at lower overpotential than Pt promoting the formation of CO₂.^[3] The amount and the local atomic configuration of these bifunctional sites (catalytic ensemble effect^[4]) play a crucial role in the catalysts' reactivity, which depends on the material's nominal composition. Furthermore, mutual modifications of the electronic properties by the foreign metal (ligand effect) modify the binding energies of the adsorbates and contribute to the resulting catalytic properties.^[5] A combination of all these effects leads to the observation that the maximum catalytic activity is not necessarily obtained for catalyst materials with a 50:50 Pt:Ru ratio and that the optimum ratio will be different for the MOR and the COOR.^[6]

In general, the COOR is considered as the rate-limiting step for the MOR.^[1a] In that context, Tritsarís and Rossmeisl determined the reactivity of various flat and stepped mono- and bimetallic surfaces making use of the concept of binding energies as reactivity descriptor (specifically for *CO and *OH binding energies) and the so-called linear scaling relations.^[7] Their results suggest a high MOR activity of Pt₈₀Ru₂₀/Ru(0001) surface alloys, which according to the authors is in qualitative agreement with the high activity observed experimentally for nanostructured catalyst materials with similar composition.^[7] Stimulated by this work, we here present experimental results for the MOR on Pt_xRu_{1-x}/Ru(0001) surface alloys prepared under ultrahigh vacuum conditions (UHV), which present very similar structural characteristics^[8] to those in the computational work introduced above. In addition we explored monolayer high Pt island modified Ru(0001) (Pt_{x-ML}/Ru(0001)) and electrochemically restructured Pt_{x-ML}/Ru(0001) electrodes to elucidate other structural parameters that possibly drive the MOR. In order to discuss possible CO poisoning effects, we included the COOR results from previous studies recorded on electrodes with similar composition and structural properties.^[6e,9]

Figure 1 and Figure 2 show the results from the electrochemical/catalytic investigations on the various Pt_xRu_{1-x}/Ru(0001) and Pt_{x-ML}/Ru(0001) electrodes. In the case of Pt_xRu_{1-x}/Ru(0001) (Figure 1), we investigated electrodes with increasing surface Pt contents (25 at.%, 35 at.% and 80 at.%). The corre-

[a] Dr. A. K. Engstfeld, Dr. J. Klein
Institute of Surface Chemistry and Catalysis, Ulm University
Albert-Einstein-Allee 47, 89081 Ulm, Germany
E-mail: albert.engstfeld@uni-ulm.de

[b] Dr. A. K. Engstfeld
Present Address:
Institute of Electrochemistry, Ulm University
Albert-Einstein-Allee 47, 89081 Ulm, Germany

[c] Dr. S. Brimaud
Zentrum für Sonnenenergie- und Wasserstoff-Forschung Baden-Württemberg (ZSW)
Helmholtzstrasse 8, 89081 Ulm, Germany

 Supporting information for this article is available on the WWW under <https://doi.org/10.1002/cphc.202000979>

 An invited contribution to a Special Collection on Interface Phenomena

© 2021 The Authors. ChemPhysChem published by Wiley-VCH GmbH.
This is an open access article under the terms of the Creative Commons Attribution Non-Commercial License, which permits use, distribution and reproduction in any medium, provided the original work is properly cited and is not used for commercial purposes.

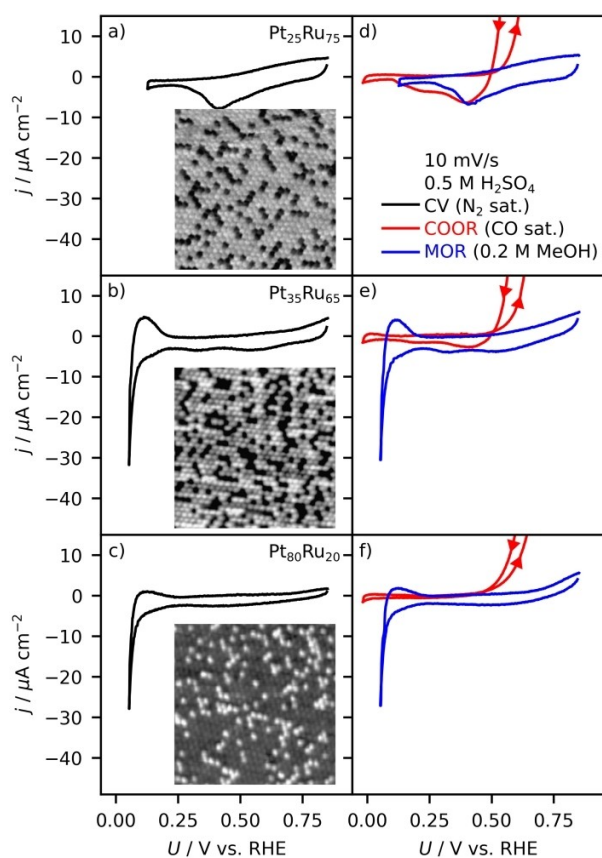


Figure 1. Electrochemical/catalytic properties of $\text{Pt}_x\text{Ru}_{1-x}/\text{Ru}(0001)$ surface alloys with increasing Pt coverage (from top to bottom). The left column shows the CVs (black curves) in plain electrolyte, and the right columns, the COOR (red curves), and the MOR (blue curves). Full COOR curves are shown in the SI. The insets show representative STM images ($7 \text{ nm} \times 7 \text{ nm}$), where Pt/Ru atoms appear as dark/bright spots (reprinted with permission from Ref. [8a]).

sponding STM images are shown in the insets, where Ru/Pt atoms appear as bright/dark spots (reprinted from Ref. [8a]). The STM images for $\text{Pt}_{x-\text{ML}}/\text{Ru}(0001)$ electrodes (Figure 2) were acquired before the MOR measurements. For $\text{Pt}_{x-\text{ML}}/\text{Ru}(0001)$, we investigated two samples with coverage of ca. 0.3 ML Pt, but different island densities and another sample with ca. 0.5 ML Pt. The structure formation and structural properties of the electrodes are described in the experimental section (see also Ref. [8], Ref [10]). In Figure 1 and Figure 2, the left columns show the cyclic voltammograms (CVs) recorded in N_2 -saturated $0.5 \text{ M H}_2\text{SO}_4$ electrolyte (black curves). The right columns show an overlay of the MOR current (blue curves) recorded in $0.5 \text{ M H}_2\text{SO}_4 + 0.2 \text{ M MeOH}$ and a part of the CO oxidation current (red curves) recorded in CO saturated $0.5 \text{ M H}_2\text{SO}_4$. All voltammograms were recorded at 10 mVs^{-1} . The full COOR curves, showing significantly higher activities than the MOR curves, are provided for comparison in the SI.

First, we briefly describe how the features in the CVs are related to the structural properties of the electrodes (see also Ref. [6a] and Ref. [9] for a detailed description). For all electrodes, the Faradaic currents observed at potentials

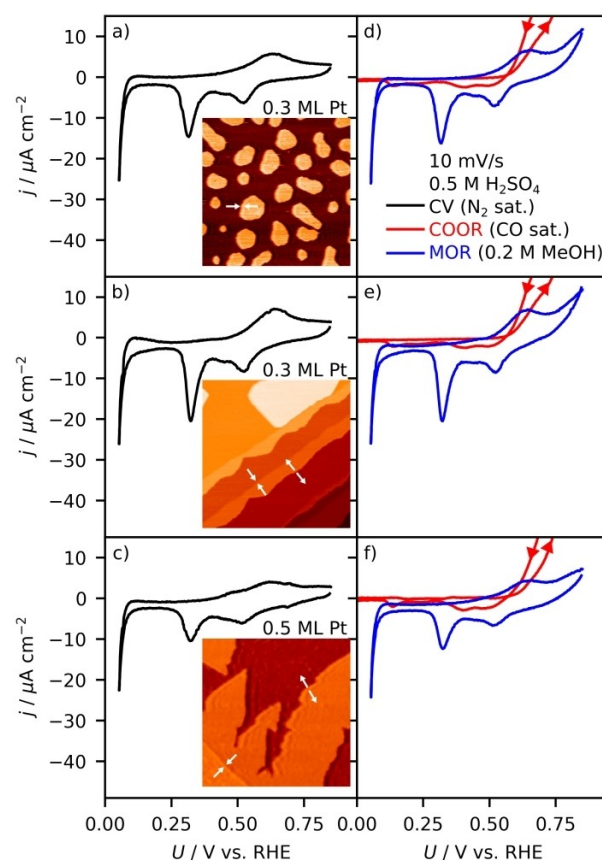


Figure 2. Electrochemical/catalytic properties of $\text{Pt}_{x-\text{ML}}/\text{Ru}(0001)$ surfaces. First and second-row show $\text{Pt}_{0.3-\text{ML}}/\text{Ru}(0001)$ electrodes with different island density, and the bottom row shows a $\text{Pt}_{0.5-\text{ML}}/\text{Ru}(0001)$ electrode. The left columns show the CVs (black curves) in plain electrolyte and the right columns show the COOR (red curves) and the MOR (blue curves). Full COOR curves are shown in the SI. The insets show representative STM images ($100 \text{ nm} \times 100 \text{ nm}$). “ \leftarrow ” and “ \rightarrow ” indicate PtRu step and interface sites.

$< 0.25 \text{ V}$ are associated with the hydrogen evolution reaction (HER) and hydrogen underpotential deposition (H_{UPD}). The oxidation/reduction peaks at potentials $> 0.25 \text{ V}$ in the positive/negative-going potential scan are attributed to the reversible formation and desorption of $^*\text{OH}/^*\text{O}$ on the Ru surface. In the case of the $\text{Pt}_x\text{Ru}_{1-x}/\text{Ru}(0001)$ electrodes, these redox features are broader compared to the $\text{Pt}_{x-\text{ML}}/\text{Ru}(0001)$ electrodes. This broadening is caused by changes in Ru sites' electronic properties induced by the incorporation of Pt atoms.^[6e]

In the positive-going COOR scan (red curve) CO poisoning suppresses the current on all electrodes at potentials $< 0.50 \text{ V}$. For $\text{Pt}_x\text{Ru}_{1-x}/\text{Ru}(0001)$ electrodes the currents increase sharply at potentials $> 0.5 \text{ V}$, reaching mass transport limitation between 0.75 V and 0.9 V , with currents around $650 \mu\text{A cm}^{-2}$ (see SI). In comparison, the $\text{Pt}_{x-\text{ML}}/\text{Ru}(0001)$ electrodes are less active than the surface alloys in the potential range investigated.^[9] Unexpectedly, the MOR studied on such electrodes (blue curves) imply that all electrodes are almost inactive since the MOR curves are almost indistinguishable from the CVs. The only difference between the MOR and the CV curves is a slight

increase of the MOR current at potentials $> \sim 0.5$ V. This becomes more apparent from Figure S4 where the CV currents are plotted together with the MOR currents. For a better comparison of the MOR activities we isolate the MOR currents by subtracting the CV currents from the MOR currents. With this we remove the contribution from other surface redox processes in the positive-going potential scan as discussed in more detail in the SI. The resulting curves are shown in Figure 3. To explain this unexpected low activity of the presented model electrodes for the MOR, we discuss in the following paragraphs systematically the influence of CO poisoning, structural effects, and electronic effects on the reaction.

Overall, CO poisoning cannot be the origin of the low MOR activity for the following two reasons. First, the COOR is sufficiently fast at potentials > 0.5 V for all electrodes. Thus, possible *CO forming as poisoning intermediate during MOR on the surface should, in fact, readily oxidize to CO_2 in this potential region. Secondly, the presence of *CO should suppress (or at least significantly lower) the H_{UPD} and the HER at potentials < 0.25 V during the MOR as it is observed for the COOR (in red), which is not the case (compare blue and black curves in Figure 1 and 2). Thus, it can be reasonably excluded that (i) the surface is significantly poisoned by *CO during the MOR and that (ii) the electro-oxidation of *CO is the rate-limiting step for the MOR on the type of bimetallic PtRu surfaces investigated in this work.

The role of different structural properties on the COOR and MOR activity is first discussed separately for the $Pt_xRu_{1-x}/Ru(0001)$ and $Pt_{x-ML}/Ru(0001)$ electrodes. Previous work shows that for the COOR all $Pt_xRu_{1-x}/Ru(0001)$ electrodes are more active than $Ru(0001)$ terminated by a Pt monolayer or pure Pt(111) electrodes, strongly suggesting that bifunctional effects drive the COOR on these surfaces.^[6e] The activity of the $Pt_xRu_{1-x}/Ru(0001)$ electrodes is directly related to the abundance of compact threefold Ru ensembles vicinal to a Pt atom (maximum activity at ca. 25–35 at.% Pt).^[6e] From the MOR curves in Figure 3 a) it seems that the activity increases slightly at potentials > 0.6 V with increasing Pt content. This possible trend should, however, not be overinterpreted. More important is that the low MOR activity apparently contradicts the classical bifunctional mechanism, computational findings,^[7] and that three-

and fourfold Pt ensembles adjacent to Ru atoms are beneficial for the MOR.^[6a-c] According to these concepts, the $Pt_{0.8}Ru_{0.2}/Ru(0001)$ electrodes were expected to be the most active surface, which were also suggested from scaling relations to be very active materials for the MOR.^[7] We expected that at least qualitative predictions from such scaling relations between experiment and theory would hold, which was for example successfully shown for the oxygen reduction reaction on well-defined electrodes.^[11]

For the $Pt_{x-ML}/Ru(0001)$ electrodes it was shown in previous studies that the COOR activity increases with increasing Pt coverage (for coverages < 1.0 ML).^[9a] In that case, the activity increase was attributed to an increase in the Pt area, with a negligible effect of PtRu step sites at the Pt islands' edges. In contrast, the MOR activity on these electrodes is negligible, even though the surface contains large Pt regions on the monolayer high Pt islands, providing three- and fourfold ensembles which were suggested to be beneficial for the dehydrogenation of MeOH.^[6a-c] Note that most of these ensembles are, however, not located adjacent to Ru atoms, except for those (i) at the interface between the monolayer high Pt islands attached to the former Ru step (PtRu interface sites) and (ii) at the perimeter of the Pt islands and the $Ru(0001)$ terrace (PtRu step sites) indicated by " $\rightarrow\leftarrow$ " and " $\leftarrow\rightarrow$ " in the STM images in Figure 2. An interesting observation from the MOR curves in Figure 3 is that the $Pt_{x-ML}/Ru(0001)$ electrodes appear to be in general more active for the MOR compared to the $Pt_xRu_{1-x}/Ru(0001)$ electrodes at potentials > 0.7 V, even though the latter contain a more considerable amount of bimetallic PtRu surface sites. We suggest that the activity is related to the different structural properties of these two types of electrodes.

In a simplified picture, the $Pt_{x-ML}/Ru(0001)$ electrode surfaces contain two types of PtRu sites; namely the interface and step sites introduced above. We assume that the PtRu interface sites do not contribute significantly to the overall activity since their flat geometric arrangement resembles that of the $Pt_xRu_{1-x}/Ru(0001)$ surfaces, which are also almost inactive for the MOR. Differently, the PtRu step sites consist of Pt atoms with lower coordination than those in a flat configuration in the surface alloys. It is well established that the very different physical properties of such low-coordinated sites contribute in different ways to gas-phase catalytic and electrocatalytic activities compared to terrace sites.^[12] In that sense, it has for example been reported that the MOR activity on stepped Pt(hkl) electrodes increases with an increasing number of Pt step sites.^[13] Furthermore, it is important to note that Ru modified stepped Pt electrodes, are active for the MOR.^[14] Based on the MOR activity of the two samples with different Pt island density and hence different amount of PtRu step sites (see blue and orange curves in Figure 3 b)) we were, however, unable to provide direct evidence that these sites contribute significantly to the overall activity. Hence either the change in the number of these sites is too low to result in a measurable current contribution or these sites are merely inactive for the reaction, possibly due to electronic effects discussed further below.

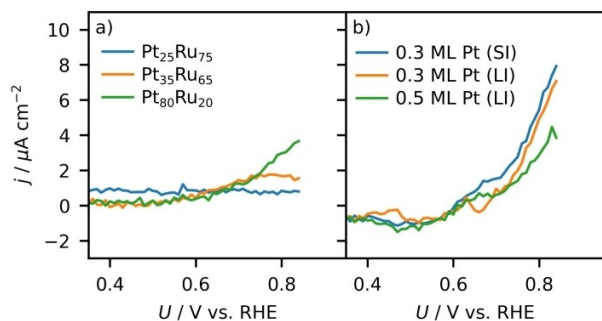


Figure 3. Comparison of the MOR activity in the positive-going scan of a) $Pt_xRu_{1-x}/Ru(0001)$ and b) $Pt_{x-ML}/Ru(0001)$ electrodes. Curves are obtained by subtracting the CV (black curves) from the MOR curves (blue) from Figure 1 and 2. SI/LI refer to surfaces with large/small islands (see text for details).

A former study also showed that the COOR activity of $\text{Pt}_{x-\text{ML}}/\text{Ru}(0001)$ electrodes significantly increases when the surface is irreversibly restructured (obtained by successive potential cycling to an upper potential limit fixed at 1.05 V).^[9] The STM images in Figure 4 a) and b) show a stable and restructured surface of a $\text{Pt}_{0.5-\text{ML}}/\text{Ru}(0001)$ electrode. The stable electrode's structural properties are similar to those on the as-prepared electrode (see inset Figure 2 c)). The small additional noisy features are residues from the electrolyte. On the restructured electrode, cluster-like structures appear within the perimeter of the original Pt islands, and Ru is removed from the former Ru step edges, revealing the Ru terrace below (marked by $\text{Ru}^\#$). The exact atomic composition/structure of the severely restructured Pt areas is, unfortunately, not accessible from our STM data. Previously we inferred that these structures are primarily formed from Pt atoms, which migrate from the monolayer islands in the second layer.^[9] Furthermore we suggested that these structures could also contain Ru atoms, resulting from re-deposition of dissolved Ru on the newly formed Pt structures. Based on a recent study on the dissolution of Ag from $\text{AgPt}/\text{Pt}(111)$ surface alloys, we suggest, however, that with a flow-cell set-up redeposition of Ru atoms is unlikely since it is more probable that dissolved species are transported away from the electrode with the flowing electrolyte.^[15] The positive-going potential scans for the COOR (red) and MOR (blue) on both stable and restructured electrodes are shown in Figure 4 c). In both cases, the restructured electrodes are more active than the stable counterparts at potentials > 0.5 V.

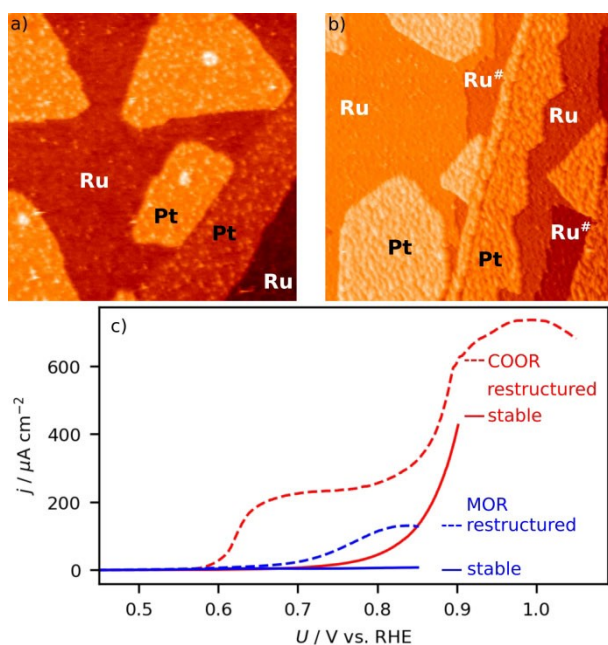


Figure 4. STM images (200 nm \times 200 nm) of $\text{Pt}_{0.5-\text{ML}}/\text{Ru}(0001)$ electrodes after potential cycling a) to 0.90 V (stable electrodes) and b) after repeated cycling to 1.05 V (restructured electrodes). Pt and Ru regions are annotated, where $\text{Ru}^\#$ denotes regions where the topmost Ru layer was removed. c) COOR (red curves) and MOR activity (blue curves) recorded on stable (solid curves) and restructured (dashed curves) $\text{Pt}_{0.5-\text{ML}}/\text{Ru}(0001)$ electrodes. The restructuring was induced by 40 potential cycles to 1.05 V (not shown).

Furthermore the MOR activity on the restructured electrodes is significantly lower compared to the COOR activity. This observation indicates that the COOR is not rate-limiting on these electrodes for the same reasons as mentioned above.

First, note that the increase in activity for restructured electrodes cannot be rationalized by an increase in Pt surface area, since the restructuring of the monolayer high Pt islands results in a decrease of effective Pt surface area. Second, we suggest that the origin of the higher activity, for the COOR and the MOR, is not attributed to a bifunctional effect at the perimeter of the Pt structures, since these sites were shown above to be rather inactive on the non-restructured electrodes. Instead we assume that the increase in activity is due to an increase in the number of Pt defect sites on the restructured Pt areas. As mentioned above, low coordinated sites on vicinal $\text{Pt}(111)$ surfaces were shown to enhance the MOR.^[13]

Finally, the low activity of the non-restructured electrodes can eventually be rationalized by electronic effects, whose impact on the adsorption properties of reactants on PtRu model electrodes has been studied widely in the past. For example, the binding energy of $^*\text{CO}$,^[16] $^*\text{O}$ ^[17] and $^*\text{H}_2\text{O}$ ^[18] on $\text{Pt}_{x-\text{ML}}/\text{Ru}(0001)$ electrodes decreases with decreasing Pt layer thickness. This trend is ascribed to a downshift of the d -band centre of the Pt atoms induced by the $\text{Ru}(0001)$ support via strain and ligand effects.^[5b,19] Based on the concept of linear scaling relations,^[7,20] we assume that this trend is also valid for MeOH and its reaction intermediates, which is discussed in detail in a study focusing on the MOR activity on Pt multilayer modified $\text{Ru}(0001)$.^[21] Furthermore, based on MeOH adsorption experiments under UHV conditions, it was shown that the thermal activation of MeOH is negligible for the first two Pt layers.^[22] Hence we propose that on the monolayer structures (surface alloys and Pt monolayer islands) both the activation barriers for the initial dehydrogenation of MeOH as well as the low binding energy of its intermediates are responsible for the low activity. Finally, note that MeOH adsorption and dissociation on clean and $^*\text{O}$ pre-covered $\text{Pt}_x\text{Ru}_{1-x}/\text{Ru}(0001)$ surfaces (similar to this work) is possible under UHV conditions.^[23] We suggest, however, that these processes might not occur or are significantly kinetically hindered under electrochemical conditions, where the surface is presumably covered by densely packed H_2O , $^*\text{O}/^*\text{OH}$, (bi)sulfate,^[24] hydrogen^[25] adlayers or even a combination of those at low potentials, acting as poison for the MeOH adsorption/decomposition.

In total, our results on the non-restructured electrodes demonstrate that the availability of bifunctional sites on a catalyst surface does not necessarily enhance the MOR activity and that $^*\text{CO}$ poisoning is not always a reasonable explanation for low activities. Furthermore, we assume that the formation of bimetallic sites on the restructured Pt areas is rather unlikely in our experiment and hence from the higher MOR activities observed on restructured electrodes, we infer that pure Pt defect sites on the newly formed Pt clusters are catalytically more relevant compared to the bifunctional sites at the perimeter of the $\text{Ru}(0001)$ supported Pt structures or the bimetallic PtRu step sites on the non restructured $\text{Pt}_{x-\text{ML}}/\text{Ru}(0001)$ electrodes.

Acknowledgements

The manuscript is dedicated to Prof. Jürgen Behm. AKE, JK and SB thank Jürgen Behm for the instructive years during their stay at his group. Open access funding enabled and organized by Projekt DEAL.

Conflict of Interest

The authors declare no conflict of interest.

Keywords: bifunctional mechanism · electrocatalysis · methanol oxidation · platinum · ruthenium

- [1] a) O. A. Petrii, *J. Solid State Electrochem.* **2008**, *12*, 609–642; b) Y. V. Tolmachev, O. Petrii, *J. Solid State Electrochem.* **2017**, *21*, 613–639; c) O. A. Petry, B. I. Podlovchenko, A. N. Frumkin, H. Lal, *J. Electroanal. Chem.* **1965**, *10*, 253–269; d) N. Kakati, J. Maiti, S. H. Lee, S. H. Jee, B. Viswanathan, Y. S. Yoon, *Chem. Rev.* **2014**, *114*, 12397–12429; e) B. Braunschweig, D. Hibbitts, M. Neurock, A. Wieckowski, *Catal. Today* **2013**, *202*, 197–209; f) M. P. Hogarth, T. R. Ralph, *Platinum Met. Rev.* **2002**, *46*, 146–164.
- [2] a) T. H. M. Housmans, A. H. Wonders, M. T. M. Koper, *J. Phys. Chem. B* **2006**, *110*, 10021–10031; b) Z. Jusys, R. J. Behm in *Methanol, formaldehyde and formic acid adsorption/oxidation on carbon-supported Pt nanoparticle fuel cell catalyst: A comparative quantitative DEMS study*, Vol. (Ed. M. T. M. Koper), Wiley&Sons, Chichester, **2009**, pp. 411–464; c) A. A. Abd-El-Latif, H. Baltruschat, *J. Electroanal. Chem.* **2011**, *662*, 204–212; d) E. Herrero, W. Chrzanowski, A. Wieckowski, *J. Phys. Chem.* **1995**, *99*, 10423–10424; e) E. A. Batista, G. R. P. Malpass, A. J. Motheo, T. Iwasita, *J. Electroanal. Chem.* **2004**, *571*, 273–282.
- [3] a) M. Watanabe, S. Motoo, *J. Electroanal. Chem. Interfac. Electrochem.* **1975**, *60*, 275–283; b) M. Watanabe, S. Motoo, *J. Electroanal. Chem. Interfac. Electrochem.* **1975**, *60*, 267–273.
- [4] a) J. W. A. Sachtler, G. A. Somorjai, *J. Catal.* **1983**, *81*, 77–94; b) J. A. Rodriguez, *Surf. Sci. Rep.* **1996**, *24*, 223–288.
- [5] a) J. W. A. Sachtler, J. P. Biberian, G. A. Somorjai, *Surf. Sci.* **1981**, *110*, 43–55; b) B. Hammer, J. K. Nørskov, *Adv. Catal.* **2000**, *45*, 71–129; c) E. Christoffersen, P. Liu, A. Ruban, H. L. Skriver, J. K. Nørskov, *J. Catal.* **2001**, *199*, 123–131.
- [6] a) R. Parsons, T. VanderNoot, *J. Electroanal. Chem.* **1988**, *257*, 9–45; b) H. A. Gasteiger, N. M. Markovic, P. N. Ross, E. J. Cairns, *J. Phys. Chem.* **1993**, *97*, 12020–12029; c) N. Markovic, H. A. Gasteiger, P. N. Ross, X. Jiang, I. Villegas, M. J. Weaver, *Electrochim. Acta* **1995**, *40*, 91–98; d) B. Du, S. A. Rabb, C. Zangmeister, Y. Tong, *Phys. Chem. Chem. Phys.* **2009**, *11*, 8231–8239; e) J. Klein, S. Brimaud, A. K. Engstfeld, R. J. Behm, *Electrochim. Acta* **2019**, *306*, 516–528.
- [7] G. A. Tritsarlis, J. Rossmeisl, *J. Phys. Chem. C* **2012**, *116*, 11980–11986.
- [8] a) H. E. Hoster, A. Bergbreiter, P. Erne, T. Hager, H. Rauscher, R. J. Behm, *Phys. Chem. Chem. Phys.* **2008**, *10*, 3812–3823; b) H. E. Hoster in *Surface Alloys*, Vol. 3 Wiley-VCH Verlag GmbH & Co, Weinheim, **2014**, pp. 329–367.
- [9] a) A. K. Engstfeld, S. Brimaud, R. J. Behm, *Angew. Chem. Int. Ed.* **2014**, *53*, 12936–12940; *Angew. Chem.* **2014**, *126*, 13150–13154; b) A. K. Engstfeld, J. Klein, S. Brimaud, R. J. Behm, *Surf. Sci.* **2015**, *631*, 248–257.
- [10] U. Käsberger, P. Jakob, *Surf. Sci.* **2003**, *540*, 76–88.
- [11] a) S. Brimaud, A. K. Engstfeld, O. B. Alves, R. J. Behm, *J. Electroanal. Chem.* **2014**, *716*, 71–79; b) S. Brimaud, A. K. Engstfeld, O. B. Alves, H. E. Hoster, R. J. Behm, *Top. Catal.* **2014**, *57*, 222–235; c) S. Beckord, S. Brimaud, R. J. Behm, *J. Electroanal. Chem.* **2017**, *819*, 401–409.
- [12] a) M. T. Koper, *Nanoscale* **2011**, *3*, 2054–2073; b) J. Klein, V. Chesnyak, M. Low, M. Schilling, A. K. Engstfeld, R. J. Behm, *J. Am. Chem. Soc.* **2020**, *142*, 1278–1286; c) L. Vattuone, L. Savio, M. Rocca, *Surf. Sci. Rep.* **2008**, *63*, 101–168; d) S. Dahl, A. Logadottir, R. C. Egeberg, J. H. Larsen, I. Chorkendorff, E. Törnqvist, J. K. Nørskov, *Phys. Rev. Lett.* **1999**, *83*, 1814–1817.
- [13] T. H. M. Housmans, M. T. M. Koper, *J. Phys. Chem. B* **2003**, *107*, 8557–8567.
- [14] E. Mostafa, A. E. A. Abd-El-Latif, H. Baltruschat, *ChemPhysChem* **2014**, *15*, 2029–2043.
- [15] S. Beckord, S. Brimaud, R. J. Behm, *Electrochim. Acta* **2018**, *259*, 762–771.
- [16] a) S. R. Brankovic, N. S. Marinkovic, J. X. Wang, R. R. Adzic, *J. Electroanal. Chem.* **2002**, *532*, 57–66; b) M. Krausa, W. Vielstich, *J. Electroanal. Chem.* **1994**, *379*, 307–314; c) A. Schlapka, M. Lischka, A. Groß, U. Käsberger, P. Jakob, *Phys. Rev. Lett.* **2003**, *91*, 016101–016104; d) P. Jakob, A. Schlapka, *Surf. Sci.* **2007**, *601*, 3556–3568.
- [17] a) M. Lischka, C. Mosch, A. Groß, *Electrochim. Acta* **2007**, *52*, 2219–2228; b) P. Jakob, A. Schlapka, P. Gazdzicki, *J. Chem. Phys.* **2011**, *134*, 224707–224710.
- [18] P. Gazdzicki, S. Thussing, P. Jakob, *J. Phys. Chem. C* **2011**, *115*, 25379–25388.
- [19] M. Mavrikakis, B. Hammer, J. K. Nørskov, *Phys. Rev. Lett.* **1998**, *81*, 2819–2822.
- [20] a) P. Ferrin, A. U. Nilekar, J. Greeley, M. Mavrikakis, J. Rossmeisl, *Surf. Sci.* **2008**, *602*, 3424–3431; b) A. Baz, A. Holewinski, *J. Catal.* **2020**, *384*, 1–13.
- [21] J. Klein, F. Argast, A. K. Engstfeld, S. Brimaud, R. J. Behm, *Electrochim. Acta* **2019**, *311*, 244–254.
- [22] P. Gazdzicki, S. Thussing, P. Jakob, *J. Phys. Chem. C* **2011**, *115*, 23013–23022.
- [23] P. Gazdzicki, S. Thussing, P. Jakob, *J. Phys. Chem. C* **2011**, *115*, 25379–25388.
- [24] N. S. Marinkovic, M. B. Vukmirovic, R. R. Adzic in *Some Recent Studies in Ruthenium Electrochemistry and Electrocatalysis*, Vol. 42 Eds.: C. G. Vayenas, R. E. White, M. E. Gamboa-Aldeco, Springer New York, **2008**, pp. 1–52.
- [25] a) S. B. Scott, A. K. Engstfeld, Z. Jusys, D. Hochfilzer, N. Knøsgaard, D. B. Trimarco, P. C. Vesborg, R. J. Behm, I. Chorkendorff, *Catal. Sci. Technol.* **2020**; b) A. M. El-Aziz, L. A. Kibler, *Electrochem. Commun.* **2002**, *4*, 866–870.

Manuscript received: December 1, 2020

Revised manuscript received: February 16, 2021

Accepted manuscript online: February 26, 2021

Version of record online: April 6, 2021